ACS APPLIED MATERIALS & INTERFACES

Research Article

www.acsami.org

Plasma Micro-Nanotextured, Scratch, Water and Hexadecane Resistant, Superhydrophobic, and Superamphiphobic Polymeric Surfaces with Perfluorinated Monolayers

Kosmas Ellinas,[†] Sidharam P. Pujari,[‡] Dimitrios A. Dragatogiannis,[∥] Constantinos A. Charitidis,[∥] Angeliki Tserepi,[†] Han Zuilhof,*[,‡,§] and Evangelos Gogolides*[,†]

[†] Institute of Nanoscience and Nanotechnology, NCSR "Demokritos", Aghia Paraskevi,153 10 Attiki, Greece

[‡] Laboratory of Organic Chemistry, Wageningen University, Dreijenplein 8, 6703 HB, Wageningen, The Netherlands

[§] Department of Chemical and Materials Engineering, King Abdulaziz University, Jeddah, Saudi Arabia

[∥] Laboratory Unit of Advanced, Composite, Nano-Materials and Nanotechnology, School of Chemical Engineering, National Technical University of Athens, 9 Heroon Polytechniou St. Zografos, 157 80 Athens, Greece

Supporting Information

ABSTRACT: Superhydrophobic and superamphiphobic toward superoleophobic polymeric surfaces of polymethyl methacrylate (PMMA), polyether ether ketone (PEEK), and polydimethyl siloxane (PDMS) are fabricated in a two-step process: (1) plasma texturing (i.e., ion-enhanced plasma etching with simultaneous roughening), with varying plasma chemistry depending on the polymer, and subsequently (2) grafting of self-assembled perfluorododecyltrichlorosilane monolayers (SAMs). Depending on the absence or not of an etch mask (i.e., colloidal microparticle self-assembly on it), random or ordered hierarchical micro-nanotexturing can be obtained. We demonstrate that stable organic monolayers can be grafted onto all these textured polymeric surfaces. After the monolayer deposition, the initially hydrophilic polymeric surfaces become superamphiphobic with static contact angles for water and oils >153°, for hexadecane >142°, and hysteresis <10° for all surfaces. This approach thus provides a simple and generic method to obtain superamphiphobicity on polymers toward superoleophobicity. Hydrolytic and hexadecane immersion tests prove that superamphiphobicity is stable for more than 14 days. We also perform nanoscratch and post nanoscratch tests to prove the scratch resistance of both the texture and the SAM and demonstrate lower coefficient of friction of the SAM compared to the uncoated surface. Scanning electron microscope observation after the nanoscratch tests confirms the scratch resistance of the surfaces.

KEYWORDS: *superamphiphobic polymers, superoleophobicity, plasma micro-nanotexturing, hydrolytic stability, scratch resistant polymeric surfaces, solvent resistant polymers, perfluorinated monolayers on polymers*

1. INTRODUCTION

A major goal of surface and coating research is to design and fabricate surfaces with special antiwetting properties, which repel not only water,[1−3] but also oils or even lower surface energy liquids (amphiphobicity (both, water + oil repellant), oleophobicity (oil repellant), omniphobicity (all-repellant) are terms used in the literature to describe the phenomenon).[4] The term superoleophobicity is commonly used when a surface exhibits high contact angle >150° and low hysteresis <10° for low surface tension liquids such as alkanes (i.e., hexadecane).[5] Nanostructuring as well as chemical modification of polymeric surfaces using low surface energy organic layers have been extensively applied toward this goal not only for open surfaces, but also in microfluidics.[6−8] Such "smart" modified polymers display a significant potential for a range of biomedical applications, in microcontact printing,[9] and facilitate the further development of "smart" multifunctional devices and systems (MEMS/NEMS).[6,10]

Although there are superhydrophobic surfaces obtained with micronanostructured materials having an initial contact angle less than 90° (on a flat surface), metastable superamphiphobic surfaces require both (a) chemical surface modification using low-surface energy molecules,[12,13] and (b) well-designed topography with re-entrant curvature structures with predesigned spacing, height, and undercut profile.[5,14−17] Zhao et al.[17] analyzed the effect of structure shape, spacing, and height in the resulting wetting properties. Tuteja et al.[5] designed a re-entrant curvature geometry using fluorinated polyhedral oligomeric silsesquioxane (POSS) as a coating material to obtain a CA for

Received: January 7, 2014
Accepted: April 21, 2014
Published: April 21, 2014

   dx.doi.org/10.1021/am5000432 | ACS Appl. Mater. Interfaces 2014, 6, 6510−6524

Figure 1. Two-step approach to obtain superamphiphobic surfaces via plasma-induced texturing and follow-up reaction with FDTS ($Cl_3SiCH_2CH_2$-$C_{10}F_{21}$).

hexadecane of ~150°. However, fabrication by this method is labor intensive and expensive. Recently, many new methods to fabricate amphiphobic/superamphiphobic surfaces are found in the literature that follow either stochastic or biomimetic bottom-up approaches,[18] or microfabrication top-down approaches.[19] Typically, these methods are done on silicon[20] or other hard substrates,[21] and little work can be found on superamphiphobic polymeric substrates. A recent review paper that includes all the progress made on superoleophobic polymers[22] stresses the need for a simple generic fabrication method that can be applied in almost any polymeric substrate (PDMS, PMMA, PEEK, and PS) with consistent results. In the current paper, we will demonstrate the development of precisely such a method.

A facile method to obtain superamphiphobic polymeric surfaces is to nanotexture polymers randomly by the use of a plasma, and subsequently deposit a fluorocarbon plasma coating.[23] To fabricate ordered, hierarchical topographies, Ellinas et al. showed that colloidal lithography followed by plasma texturing of the polymer and fluorocarbon plasma deposition can be used.[24] This yields a repellant PMMA surface, exhibiting 168°, 153°, and 134° static CAs for water, diiodomethane, and soya oil, and hysteresis 2°, 9°, and 15°, respectively. However, the static contact angle measured with hexadecane was 'only' 101°, due to the nonminimized surface energy of the C_4F_8 plasma coating. This example showed that while plasma treatment is a generic technique toward superoleophobicity of polymeric surfaces, further improvements are required in order to obtain also high CAs toward low surface tension liquids.

In contrast to disordered fluorocarbon coatings with typical surface energy values of 18.5 mN/m (the surface energy for polytetrafluoroethylene (Teflon)),[25] much lower surface energies (down to 5.6 mN/m) have been reported for ordered, perfluorinated monolayers, e.g., on Si(111) surfaces.[13,26] To make use of this feature, perfluoroalkyl monolayers[29] have been used for superoleophobic Si-containing inorganic surfaces[17,27,28] or polymers.[30,31]

An insufficient coating stability and durability usually limits the successful commercial application of superhydrophobic/superamphiphobic surfaces. Recent studies of superhydrophobic/superoleophobic surfaces have focused on the stability against capillary forces present at wetting and drying,[23,32] abrasion resistance by sand blasting,[33] or wear cycles of fabrics[34] and other characterization techniques.[35] The nanoscratch test is another well-established method to characterize the scratch resistance and the wear resistance of various surfaces or coatings,[36,37] and was recently applied to randomly plasma-nanotextured PMMA surfaces with a plasma-deposited fluorocarbon coating.[38]

In the current paper, we combine for the first time plasma-induced texturing of polymeric surfaces with a covalently attached perfluorinated monolayer (see Figure 1). The resulting data show that superamphiphobicity can be produced on polymeric surfaces using a simple and generic technology suitable for most polymers. The resulting stochastic or ordered surfaces are characterized in detail by IR spectroscopy and XPS analysis. Static CAs and hysteresis are measured for a variety of liquids, ranging from water to hexadecane and soya oil, not just for freshly prepared samples, but also after prolonged (>14 days) immersion in water or hexadecane, demonstrating for the first time the high hydrolytic and solvent immersion stability. In addition, water immersion tests are reported for up to 40 days. Furthermore, newly designed nanoscratch experiments are presented probing the texture and the monolayer, which show the scratch resistance of the textured surface and of the FDTS monolayer coating.

2. EXPERIMENTAL SECTION

2.1. Materials. Optically transparent 2-mm-thick PMMA plates were purchased from IRPEN (Spain), and opaque gray 1.5-mm-thick PEEK plates from RTP Company (USA). Both were cleaned using isopropyl alcohol (IPA) and deionized (DI) water prior to plasma processing. PDMS prepolymer was mixed with its curing agent and a thickness of ~15−20 μm was coated on silicon wafer. 1*H*,1*H*,2*H*,2*H*-Perfluorododecyltrichlorosilane (FDTS, 97%, Aldrich) was used as received. Cyclohexane CHROMASOLV Plus, for HPLC, ≥99.9% was purchased from Aldrich. Polysterene spheres of 1 and 3 μm diameter were purchased from microParticles GmbH and used as described elsewhere.[24,39]

2.2. Plasma-Induced Texturing of Polymers. Plasma processes were performed in the Micromachining Etching Tool (MET) from Alcatel at NCSR Demokritos, equipped with a helicon source (at 13.56 MHz) providing RF power up to 2000 W. Typical values for the O_2 plasma used in the texturing of organic polymers were 1900 W, 0.75 Pa, 100 sccm, −100 V bias voltage, 15 °C. Surfaces after O_2 plasma treatment became amphiphilic. The same reactor was also used for the inorganic polymer texturing using SF_6 chemistry at conditions 1900 W, 1.33 Pa, 172 sccm, 15 °C, −100 V bias voltage. Texturing is mainly formed due to the anisotropic etching conditions and the simultaneous codeposition of minute amounts of alumina molecules sputtered from the alumina helicon reactor dome (surface Al concentration after etching is 1−10% depending on the etching time).[40] Alumina is unetchable in oxygen or SF_6 plasmas, and when present in trace amounts, it initiates the formation of "nanograss"-like structures locally, which grow gradually higher since alumina preferentially sticks to the protruding parts of the topography, causing a roughness instability, as discussed in detail elsewhere.[41] The same texture and thus the same wettability is observed in samples that are processed on different dates over a period of several years with less than 10% variability. In fact, monitoring the texturing time needed to obtain CA larger than 150° and hysteresis less than 10° (this time in our case is 1 min) and monitoring the etching rate are good indicators for process and morphology repeatability or plasma reactor failures.[40,42−45] Similar texturing results have also been observed by other authors.[46,47] For long plasma treatments, the resulting filamental nanostructures are not mechanically stable. To stabilize the PEEK and PMMA surfaces before hydrophobization, the surfaces were immersed into water and upon drying the nanofilaments coalesced in shorter, more compact hierarchical microhills, due to capillary forces. Wetted−dried surfaces are mechanically stable and described elsewhere.[23] PDMS surfaces are stabilized during the silanization step, and there is no need for water immersion (see Supporting Information Figure S3 and section 3.2.3). To produce ordered hierarchical surfaces, polystyrene microspheres are spin-coated on polymer surfaces resulting in hexagonally packed

microsphere arrays. The same plasma processes as before are performed, followed by a short isotropic oxygen plasma etching step to produce undercut profiles, as described in detail elsewhere.[24] These surfaces do not need additional water-immersion stabilization.

All the fabricated surfaces exhibited re-entrant-like curvature, because of the randomly curved microhills (PMMA, PEEK), the undercut produced in the interface of the PS particle and PMMA in the ordered pillars, or the bent filamental topography of PDMS after grafting (see also SI Figure S3).

2.3. Substrate Reactivation. Since the plasma texturing took place in Athens, and the follow-up SAM preparation was always performed in Wageningen several weeks later, a brief air plasma reactivation of the surface was necessary in order to regenerate OH or COOH groups lost due to aging.[40] To this aim, a polymeric substrate was placed in the plasma reaction chamber (PDC-002 (plasma cleaner) PDC-FMG-2 (plasmaFlo), Harrick Scientific Products, Inc. Ossining, NY). The reaction chamber was pumped down to less than $(1.2 \pm 0.2) \times 10^{-2}$ mbar prior to the introduction of air plasma. Pieces of polymeric substrates were placed in the plasma cleaner and oxidized for 2 min with 0.3 SCFH air flow, 29.6 W power, at 300 mTorr pressure.

2.4. SAM Preparation. Polymeric substrates were degreased by immersion for 2 min in an ultrasonic bath containing ethanol, and then allowed to dry in a stream of argon, and reactivated in the plasma as described in section 2.3. Immediately after removal from the plasma cleaner these activated substrates were immersed for 60 min in a solution of 1 mM FDTS in cyclohexane, thoroughly rinsed with cyclohexane and dried in a stream of dry argon. Evidence for the successful surface modification was obtained from a detailed surface characterization.

2.5. Contact Angle Measurements. Contact angle analysis was performed with a Krüss DSA 100 Contact Analyzer System. Static contact angle were measured using typically 5 μL droplets. Advancing and receding angles were measured as the droplet volume was continuously increased and decreased, to estimate contact angle hysteresis. The contact angle was determined with the software suite and via graphical fitting of the contact tangents method-2 (polynomial method) in the captured image. Both approaches gave the same nominal value, typically within 1°, and always within ±2°. For each sample, at a minimum, four different readings in different spots on the surface were recorded.

2.6. Surface Characterization. An X-ray photoelectron spectrometer (XPS; JEOL JPS-9200 photoelectron spectrometer) was used, with a monochromatized Al Kα X-ray source operated at 12 kV and 20 mA. Photoelectrons were collected at a takeoff angle of 80° relative to the sample surface. Wide-scan survey spectra were acquired using a analyzer pass energy of 100 eV and a step size of 1 eV. To avoid any surface charging of the polymer surface, a charge neutralizer was employed at a setting of 5.1 A and 2.8 V. Atomic and mass percentages were calculated from the areas of representative elemental peaks using the library of relative sensitivity factors provided by the manufacturer. After a linear-type background subtraction, the raw spectra were fitted using nonlinear least-squares fitting program adopting Gaussian−Lorentzian peak shapes for all the peaks. The atomic compositions were evaluated using sensitivity factors as provided by Casa XPS v 2.3.15 software.

Attenuated total reflectance infrared (ATR-IR) spectra were collected with an α ALPHA-P Bruker equipped with an exchangeable QuickSnap sampling and platinum ATR single reflection diamond ATR module. All spectra were built up from 150 scans (resolution: 1 cm^{-1}), and referenced to a clean plasma-activated polymer surface.

2.7. Hydrolytic and Hexadecane Immersion Stability Tests of the Monolayers. We carried out the water stability experiments by placing the modified polymer surfaces inside a tailormade glass beaker, which has two connections, one for fresh deionized (DI) water 2000 mL/day (25 °C), and another for draining (see circulating water bath Figure S4 in Supporting Information). Samples remained in the bath for a predetermined period, and then were removed for contact angle measurement. In all cases, the surfaces were rinsed with fresh deionized water and ethanol, dried in a flow of dry argon, and subjected to vacuum (~10 mbar) for 30 min before the CA was measured. Water, soya oil, and hexadecane CA and hysteresis were measured. Samples were then returned to the same circulating water bath for monitoring of the stability for a longer period. In the case of hexadecane immersion, hexadecane was continuously agitated at 25 rpm using an incubator shaker and temperature was again kept constant at 25 °C.

2.8. Scratch Resistance Characterization Using Various Nanoscratch Protocols. A nanoindentation system was used to evaluate the scratch resistance of textured surfaces and to measure the coefficient of friction (CoF). The CoF is obtained as the ratio of the recorded lateral force over the applied normal load. All measurements have been performed with the standard three-side pyramidal Berkovich probe, with an average radius of curvature of about 100 nm. The indenter is a diamond with elastic modulus 1140 GPa and Poisson ratio 0.07. More details about the system used and the corresponding analysis of the data have been reported elsewhere.[48,49]

Two scratch experimental protocols were used: One duplicate scratch with steady load, and another single scratch with an increasing load. Both comprise three main segments, namely, prescan, scratch, and postscan. Prescan and postscan under a very small load (1 μN) were conducted to get an image of the surface profile before and after the scratch, respectively.

During the steady load scratch experiment, the indenter follows the loading protocol presented in Figure 2. At the beginning, a small load

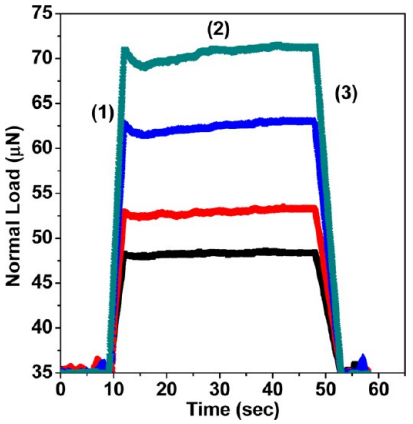

Figure 2. Scratch and postscratch load protocol: (1) preload, (2) constant load stage (for various maximum loads 10−100 μN), and (3) unloading. Different colors represent different applied loads: dark cyan corresponds to 70 μN, blue to 62 μN, red to 52 μN, and black to 47 μN.

of 35 μN is applied for 10 s, then the load is increased to the preferred value for approximately 40 s, and finally it is decreased again to 35 μN for another 5 s. The length of the scratches was 10 μm, and thus a typical scan speed was approximately 10 μm/min. A scratch cycle consists of two passes following the same protocol along the same motion path (i.e., a scratch and a post scratch over the same line) The reason for doing a duplicate scratch test over the same path is to evaluate the endurance of the coating and structures in two consecutive, repeated wear cycles. Each scratch experiment was repeated 3 times over different regions of the sample spaced 20 μm apart. Scratch tests were performed for various loading rates, constant maximum applied loads between 10 and 100 μN, and sliding speeds. We note that this scratch protocol is designed to probe the scratch resistance of the coating as well as the texture by using a constant force and thus gives complementary information to the nanoindentation tests performed before.[38]

The second protocol comprised a longer scratch (40 μm) with increasing load from 0 to 100 μN, resulting in increased penetration. It was done to explore the effect of increasing load on the structure stability. The selection of the maximum load was dictated from the penetration depth (continuously monitored during the scratch), and

from the maximum stresses developed compared to the strength of the material. Indeed, the maximum penetration depth was chosen to be less than ~850 nm to make sure that the tip does not go deeper than the height of the microstructures. The maximum stresses should be below the elastic modulus/yield strength of the material, and/or critical loads: Indeed, when a load is applied on a micropillar, pillar destruction, bending, or buckling may occur. For a given pillar geometry (e.g., diameter ~300 nm and height ~1000 nm, see Figure 5a), we calculated the maximum vertical stress caused by a 80 μN load to be approximately 1.1 GPa, well below PMMA elastic modulus $E_{\text{bulk PMMA}}$ ~5.6 GPa. In addition, the maximum bending stress at the base of the same pillar during the nanoscratch experiments due to a horizontal force of 40 μN (assuming a coefficient of friction of 0.5 and a vertical load of 80 μN) is approximately 2.6 GPa also below $E_{\text{bulk PMMA}}$ ~5.6 GPa. Finally, the critical buckling load for this PMMA pillar was calculated approximately 100 μN, dictating our choise of maximum load. Details about the theoretical formulas used for the calculations of the bending stress, and critical buckling force has been reported elsewhere.[50]

3. RESULTS AND DISCUSSION

3.1. Perfluorododecyltrichlorosilane Monolayer on Flat Polymer Surfaces. Flat fluorinated polymer surfaces were for PMMA, PEEK, and PDMS surfaces obtained by a few minutes of (low-pressure) air plasma activation of the polymers, directly followed by reacting the oxidized (−OH, −CHO, and −COOH functionalized) surfaces for 1 h with a solution of FDTS (1 mM, dry cyclohexane). In the remainder of the text, we consider as flat a surface that is not textured, and is only activated for a few minutes by air plasma, but has NOT been treated in the high-density plasma reactor. Such a brief treatment typically yielded the formation of a flat fluorinated monolayer upon a single immersion in a FDTS solution, as indicated below.

3.1.1. Characterization of the Modified Flat Surfaces: XPS and IR. To characterize in detail the variation in the surface chemistry of the substrates—untreated, air plasma-activated, and FDTS-grafted flat PDMS, PMMA, and PEEK substrates—they were analyzed by X-ray photoelectron spectroscopy (XPS). The XPS-based elemental analysis showed a decrease in the carbon composition at the surface after plasma activation and a clear increase of the oxygen content. This confirms the surface oxidation of the substrates. At this stage, no visible F signal is present on any of the polymers. Upon subsequent grafting of FDTS, fluorine appears in the XPS data in line with monolayer attachment (see Table 1, and Supporting Information Figure S1). The percentage of Si on PDMS substrates before and after plasma treatment remains approximately the same, while upon grafting of FDTS it is slightly decreased, in line with the formation of a signal-attenuating overlayer, i.e., the fluorinated monolayer (see Supporting Information Figure S1). These data are analogous to data in the literature.[40]

Peak-fitted narrow-scan C1s spectra of FDTS-modified PEEK, PDMS, and PMMA are shown in Figure 3a,c,e. A large shift (typically on the order of several eV) toward higher binding energies was typically observed in these XPS measurements due to surface charging of the polymer surfaces during the analysis. Therefore, all measurements required the use of a charge neutralizer, and the spectra were calibrated afterward by setting the major C−C/C−H peak at 285.0 eV (PDMS and PMMA) and 284.7 eV (PEEK).[51]

The composition of all three modified surfaces was also confirmed in more detail by narrow scan C1s XPS measurements. The deconvolution of the C1s signal for the FDTS-functionalized PEEK revealed the contributions of seven main carbon signals. The main C1s signal is centered at 284.7 eV and was assigned to the contribution of aromatic C−C bonds together with C═C and Si−C carbon atoms. The chemical shifts relative to this peak were quoted in parenthesis. The contributions of C1s electrons from C−O groups and $\underline{C}H_2$−CF_2 at 286.2 eV (ΔE = 1.5 eV) were too close together to be resolved and therefore were summed together. The peak at 287.2 eV (ΔE = 2.5 eV) was attributed to carbonyl carbon, while the small component at 289.2 eV is a characteristic shakeup satellite due to the π-π^* transitions in aromatic groups. The signals and their corresponding percentage with high binding energies were assigned to the $\underline{C}F_2$−CH_2 at 290.7 eV (ΔE = 6.0 eV), $\underline{C}F_2$ at 291.8 eV (ΔE = 7.1 eV), and terminal -CF_3 groups at 294.0 eV (ΔE = 9.3 eV) (Figure 3a). The relative concentrations (%) of the peaks for FDTS-grafted PEEK are (C−H/C═C, Si−C) 48.2%, $\underline{C}H_2$−CF_2 3.6%, and $\underline{C}$−O 16.5%, the π-π^* shakeup satellite 1.9%, $\underline{C}F_2$−CH_2 2.9%, CF_2−$CF_{2/3}$ 23.7%, and the CF_3 3.1%.

For FDTS-modified PDMS, the C1s XPS spectrum was deconvoluted into five components (Figure 3c), with the chemical shift relative to the (C−H/C−C, Si−C) contribution and their percentage quoted in parentheses. Hydrocarbon C atoms (C−H/C−C, Si−C) were found at 285.0 eV (ΔE = 0 eV, 37.3%), $\underline{C}H_2$−CF_2 at 286.6 eV (ΔE = 1.6 eV, 5.3%), $\underline{C}F_2$−CH_2 at 291.2 eV (ΔE = 6.2 eV, 5.7%), CF_2−$CF_{2/3}$ at 292.0 eV (ΔE = 7.0 eV, 45.9%), and the terminal CF_3 moieties at 294.1 eV (ΔE = 9.1 eV, 5.7%), as shown in Figure 3b.

The C1s deconvoluted spectrum of the FDTS-grafted PMMA substrate in Figure 3e represent the contributions of the C1s electrons from hydrocarbon (C−C/C−H and Si−C) at a binding energy of 285.0 eV (ΔE = 0 eV, 47.4%), with α-shifted carbon (C−C═O) and the $\underline{C}H_2$−CF_2 contributions summed together and found at 286.4 eV (ΔE = 1.4 eV, 14.6%). The methoxy group contribution is found at 287.5 eV (ΔE = 2.5 eV, 5.7%), while the carbonyl carbon in the ester group has a binding energy of 290.0 eV (ΔE = 5.0 eV, 6.2%). The components at 291.0 eV (ΔE = 6.0 eV, 2.8%), 292.0 eV (ΔE = 7.0 eV, 20.7%), and 294.2 eV (ΔE = 9.2 eV, 2.6%) were assigned to the $\underline{C}F_2$−CH_2, $\underline{C}F_2$−$\underline{C}F_{2/3}$, and $\underline{C}F_3$ groups, respectively.

Table 1. XPS-Based Elemental Composition[a] of Untreated, Plasma-Activated, and FDTS-Grafted Flat PMMA, PDMS, and PEEK Substrates[b]

substrate	PMMA	PDMS	PEEK
	Untreated		
%C	74.3 (71.5)	46.5 (50)	87.6 (86.4)
%O	25.7 (28.5)	24.6 (25)	12.4 (13.6)
%Si	--	28.9 (25)	--
	Plasma-Activated		
%C	65.9	18.5	79.7
%O	34.1	52.1	20.3
%Si	--	29.4	--
	FDTS Grafted		
%C	54.3	24.9	55.2
%O	11.1	25.5	9.3
%Si	3.0	18.0	1.8
%F	31.6	31.1	33.8

[a]See for survey scan XPS spectra the Supporting Information (Figure S1). [b]Theoretical composition of untreated substrates is shown in parentheses.

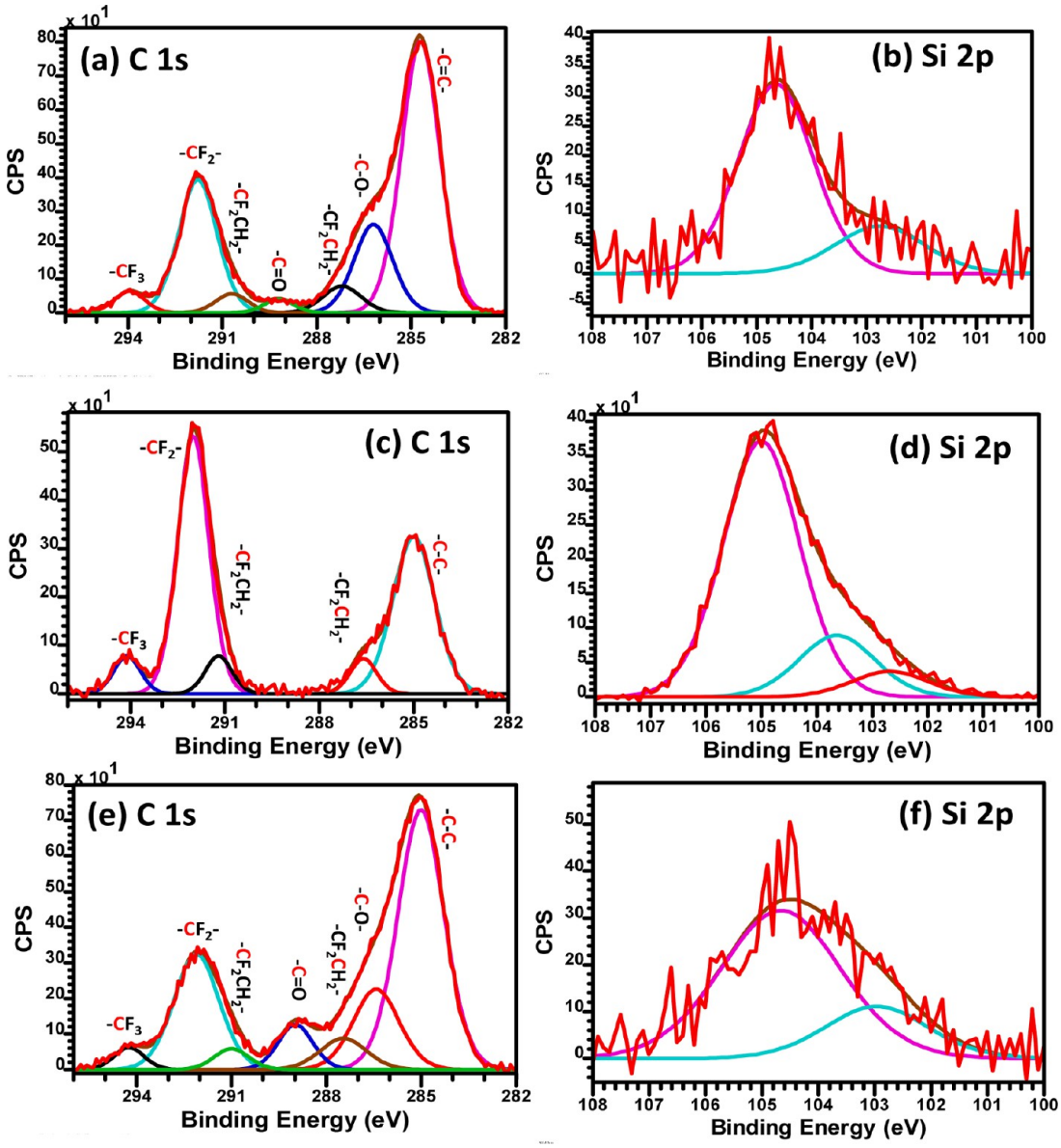

Figure 3. Peak-fitted C1s and Si2p XPS spectra of FDTS-modified PEEK (a and b), PDMS (c and d), and PMMA (e and f).

To estimate the relative coverage of these monolayers, one can compare the contribution of the clearly distinguishable contribution of the CF_3 group (one of the 12 C atoms of FDTS) with signals characteristic of the polymer. If one of those CF_3 groups would be bound per polymer repeat unit on the surface (5 C for PMMA, 2 C for PDMS, and 19 C for PEEK), then the CF_3 peak would constitute 5.8% on PMMA, 7.1% on PDMS, and 3.2% on PEEK. In fact, the CF_3 contributions amount to 2.6% on PMMA, 5.7% on PDMS, and 3.1% on PEEK. This implies a somewhat denser monolayer formation on PDMS and PEEK than on PMMA.

To confirm the presence of Si−O, Si−C, and O−Si−O bonds, the Si2p XPS peak was deconvoluted (Figure 3b,d,f) into two components at 102.7 eV (Si−C) and 104.6 eV (Si−O), respectively, in accordance with the incorporation of a silane on the PEEK and PMMA interfaces (Figure 3b and f, respectively). The experimental ratios of these two components (Si−O and Si−C) are 3.1:1, in close agreement with the theoretical ratio of 3:1. The deconvoluted Si2p XPS peak of FDTS-grafted PDMS revealed three contributions (Figure 2d). They were assigned to O−Si−O Si atoms at 105.0 eV, Si−O at 103 eV, and Si−C at 102.7 eV. The XPS narrow scans of the O1s and F1s regions further supported the successfully grafted polymer substrates (see Supporting Information, Figure S1).

The successful formation of an FDTS overlay was also confirmed by IR spectroscopy (see Supporting Information, Figure S5). This revealed the appearance of not only characteristic C−H stretching vibrations (especially clear on PMMA), but also characteristic C−F absorptions in the 1130−1250 cm^{-1} region.[52]

3.1.2. Wettability of Flat Untreated, Plasma-Activated, and FDTS-Grafted Polymer Surfaces. Contact angle (CA) measurements are sensitive indicators of the surface properties of a monolayer. The obtained monolayers on flat surfaces were analyzed with static CA measurements and a variety of test liquids, namely, water (γ_{lv} = 72.1 mN m^{-1}), soya oil, and hexadecane. Low-surface-tension liquids such as hexadecane (γ_{lv} = 27.5 mN/m) and soya oil (γ_{lv} = 34.1 mN/m) were chosen as probe liquids to observe the oleophobicity on the surface. Data for all relevant samples are summarized in Table

dx.doi.org/10.1021/am5000432 | ACS Appl. Mater. Interfaces 2014, 6, 6510−6524

2. Before modification, these surfaces were thoroughly rinsed in pentane and dried in an argon stream. The native PDMS had a water CA of 114°, while water contact angles of 82° and 60° were found for native PEEK and PMMA, respectively. Upon plasma-activation, these values drop to <40°, which confirms the formation of hydroxyl and carboxyl groups. After silanization, the water contact angles increased, to 125° for PMMA, 123° for PDMS, and 119° for PEEK. Such values are in line with the attachment of a fluorinated monolayer,[13,28,53−55] imply the presence of weak dipole−dipole interactions between the CF_3 terminus and water molecules and are slightly increased from the small nanoroughness created during the plasma activation step (see AFM images in Supporting Information Figure S2). In comparison, a PTFE surface displays a lower static water CA (typically ∼115°),[56] mainly because the CF_2 groups are less capable of reducing the surface energy than CF_3 groups.[57] The lower polarizability of fluorine compared to hydrogen leads to weak van der Waals interactions among the CF_3 terminus and polar water molecules.[13,58,59] The differences between the different polymer surfaces are attributed to the effects of differences in the AFM-observed surface roughness PMMA, 1.7 nm; PDMS, 6.7; and PEEK, 5.5 nm (AFM images of the surfaces before, after the air plasma activation, and after the grafting are shown in Figure S2 of the Supporting Information). The degree to which the polymer is swelled by cyclohexane, i.e., the solvent in which the FDTS attachment takes place, which affects the degree of fluorination. After coating with FDTS, the polymer surfaces became repellent to soya oil and water, and contact angles for hexadecane became ≥75° for all surfaces.

Table 2. Static Contact Angle and Hysteresis Data on Flat PMMA, PDMS, and PEEK before and after Silanization[a]

	PMMA	PDMS	PEEK
bare surface (water)	60°	114°	82°
soon after air plasma activation (water)	40°	25°	25°
	After Silanization		
water	125° (15°)	123 (17°)	119° (18°)
soya oil	90°	87°	92°
hexadecane	75°	76°	76°

[a]Hysteresis is shown in parentheses; experimental error: ±2°.

These high contact angle values for the flat surfaces can be attributed to the high amount of CF_3 present on surfaces after the grafting with FDTS, combined with the excellent adhesion of the coating and the slight increase of the nanoroughness during the activation step compared to flat silicon surface that exhibits water static contact angle of 120°.[13]

This excellent and conformal attachment of FDTS to our surfaces is highlighted from XPS data that show a high amount of CF_3 present (section 3.1.1), and from the CoF (coefficient of friction) data shown in section 3.3.3, which highlight that the coating is not detached or delaminated after the scratch experiments.

3.2. Wettability of Textured Polymer Surfaces. In this section, we discuss the superhydrophobic and superamphiphobic properties of the polymeric surfaces that were textured in a hierarchical manner—either randomly or in an ordered fashion—using plasma-induced texturing (see section 2.2.),[24,40,43] and subsequently coated with a perfluorosilane-based monolayer.

3.2.1. Random Textured PMMA and PEEK Surfaces. Oxygen plasma etching was used to micro-nanotexturize PMMA and PEEK surfaces, yielding a high-aspect-ratio, random re-entrant-like topography.[40] However, this topography is not stable upon immersion in water and drying, and eventually yields coalesced microhills.[23] Figure 4 shows PEEK and PMMA surfaces after texturing with O_2 plasma for 20 min, immersion in water, drying, and subsequent plasma-induced reactivation and grafting by FDTS. The PMMA surface is affected during silane modification (swells slightly in cyclohexane), yielding small changes in the morphology, and is probably accompanied by penetration of monolayer-forming silanes into the swelled polymer. In contrast, PEEK is not attacked by cyclohexane.

The dynamic contact angle measurements on the re-entrant-like micro-nanotextured PMMA and PEEK after 20 min O_2 plasma treatment and subsequent FDTS grafting are provided in Table 3. This represents a significant improvement compared to plasma-deposited fluorocarbon coatings (using C_4F_8 plasma[23]). The findings of the current study are consistent and competitive to superoleophobic surfaces reported in the literature;[27] Li et al.[60] fabricated fluorocarbon grafted cellulose

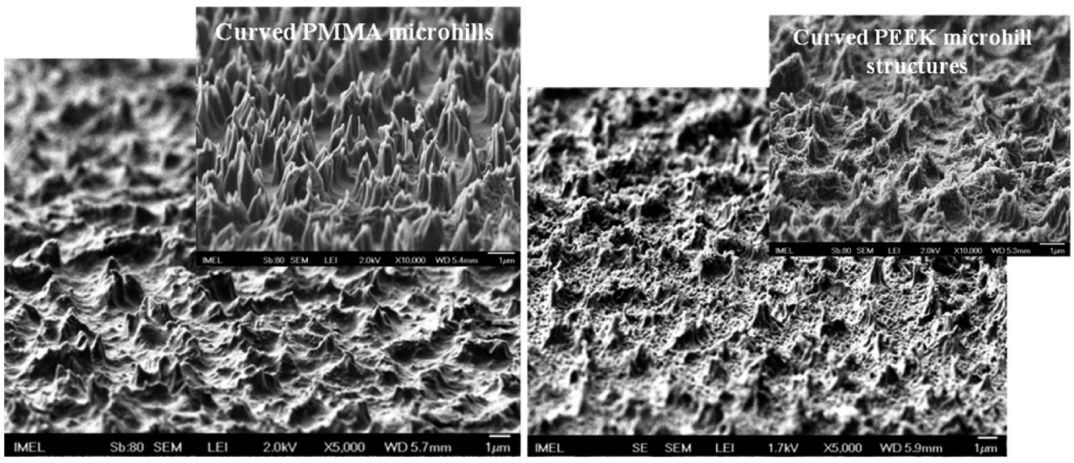

Figure 4. SEM images of micro-nanotextured, water-immersed, and dried PEEK (right) and PMMA (left) surfaces after perfluorosilane modification in cyclohexane (70° tilted). Curved, negatively sloped microhills are produced after texturing and grafting of the polymeric surfaces.

Table 3. Static, Advancing, Receding Contact Angles and Hysteresis (all in degrees) for Water, Soya Oil, and Hexadecane on Silane-Modified, Hierarchical Randomly Rough Surfaces of PMMA and PEEK[a]

liquid	contact angle	PMMA 20 min O_2 plasma	PEEK 20 min O_2 plasma
water (γ_{lv} = 72.1 mN m^{-1})	static	167°	168°
	adv/rec (hyster)	168°/166° (2°)	168°/166° (2°)
soya oil (γ_{lv} = 34.1 mN m^{-1})	static	157°	159°
	adv/rec (hyster)	157°/153° (4°)	159°/145° (14°)
hexadecane (γ_{lv} = 27.5 mN m^{-1})	static	142°	138°
	adv/rec (hyster)	145°/135° (10°)	142°/131° (11°)

[a]5 μL liquid, uncertainty in static CA, ±2°; receding CA, ±5°.

Table 4. Contact Angle Measurements for Water, Soya Oil, and Hexadecane on Silane-Modified Hierarchical Ordered PMMA Surfaces with PS Microparticles[a]

liquid	contact angle	1 μm PS on PMMA (Figure 4a) 1 min 30 s (anisotropic) + 30 s (isotropic)	3 μm PS on PMMA (Figure 4b) 4 min 30 s (anisotropic) + 1 min 30 s (isotropic)
water	static	166° [165°]	167° [168°]
	adv/rec	168°/166° (2°) [≤2°]	168°/164° (4°) [≤5°]
soya oil	static	153° [125°]	154° [134°]
	adv/rec	159°/152° (7°)	157°/150° (7°) [>15°]
hexadecane	static	140° [96°]	142° [101°]
	adv/rec	142°/133° (9°) [>30°]	143°/133° (10°) [>30°]

[a]Hysteresis is shown in parenthesis for adv/rec measurements. 5 μL liquid, uncertainty in static CA, ±2°; receding CA, ±5°. Note: The corresponding contact angles and hysteresis when a plasma-deposited fluorocarbon layer was used instead of the current FDTS grafting are shown in [square brackets], to reveal the improvement using the FDTS monolayer compared to ref 24.

that exhibited hexadecane CA 152°. High static and low hysteresis angles for all the tested liquids are attributed to the random, curved, negatively sloped microhill topography produced after texturing and grafting.

3.2.2. Ordered Hierarchical Micronanotextured PMMA Surface. Figure 5 shows SEM images of uniform, mushroom-like micropillars produced on PMMA by the combination of colloidal lithography using PS particles and plasma etching as described before.[24] These mushroom-like re-entrant micropillars do not display any coalescence after immersion in water or silane solvent solution for 1 h. High-resolution SEM images of surfaces show the same morphology before and after silanization (see Supporting Information Figure S3).

The contact angle results are shown in Table 4 for FDTS-modified, ordered (using both 1 and 3 μm PS particles) PMMA surfaces. In addition, this table presents the comparison with contact angles from our previously reported work[24] (in brackets) using the same re-entrant topography with the C_4F_8 plasma-deposited layer (film thickness 30 nm). In all cases the current CAs with water, soya oil, or hexadecane are higher to significantly higher than previous results. This highlights the efficient functionalization with FDTS, which results in a high local CF_3 density concentration that yields a superhydrophobic material with a low surface energy.

The contact angle hysteresis values are for water <4°, for soya oil ~7°, and for hexadecane ~10°. Such values indicate a Cassie or impregnating Cassie state. Water and soya oil drops (5 μL) roll off easily from these surfaces, by tilting only ~1° for water and <8° for soya oil. The rolling-off movements were captured in videos (see Supporting Information).

We used the same optimized topography with our recent work[24] to highlight the improvement in the CA due to the different coating used. This improvement is probably caused by the higher CF_3 amount present in the FDTS coating compared to the plasma deposited C_4F_8, and a better adhesion and conformal deposition of the FDTS coating (see also sections 3.1.1 for XPS and IR and section 3.3.3 for the CoF of the FDTS coating).

3.2.3. Random Textured PDMS Surfaces. SF_6 plasma etching was used to texture PDMS surfaces, resulting in a high aspect ratio topography. The resulting topography after 10

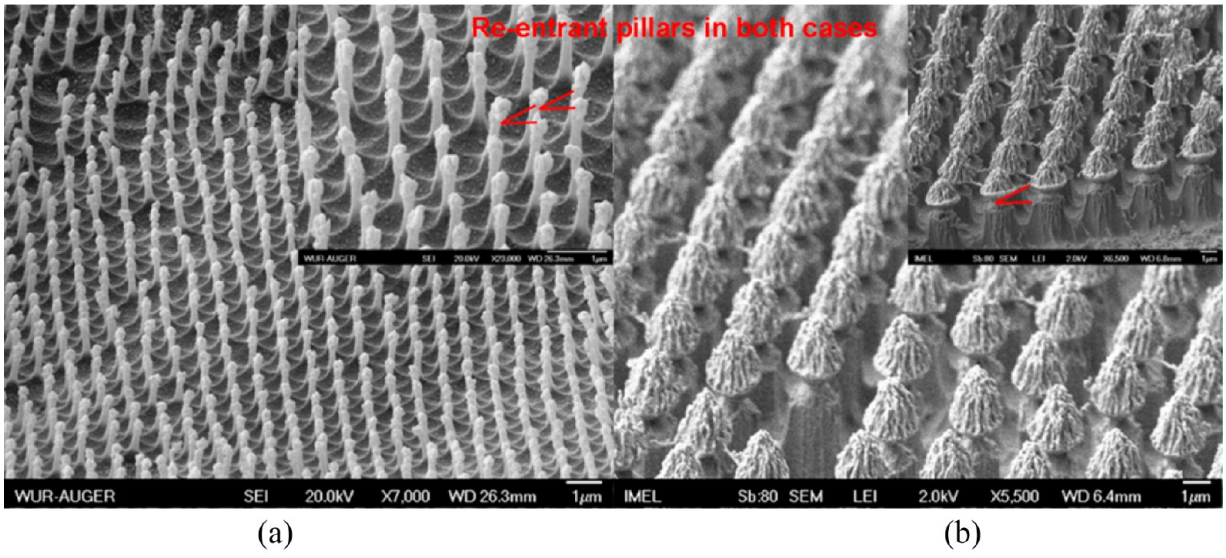

Figure 5. SEM images of PMMA surfaces (60° tilted) displaying the hierarchical, hexagonically ordered packed pillars obtained upon plasma etching using (a) 1 μm and (b) 3 μm polystyrene particles. Notice the undercut produced in both cases (re-entrant pillars) using the optimized process proposed elsewhere.[24] CA for each case is shown in Table 4.

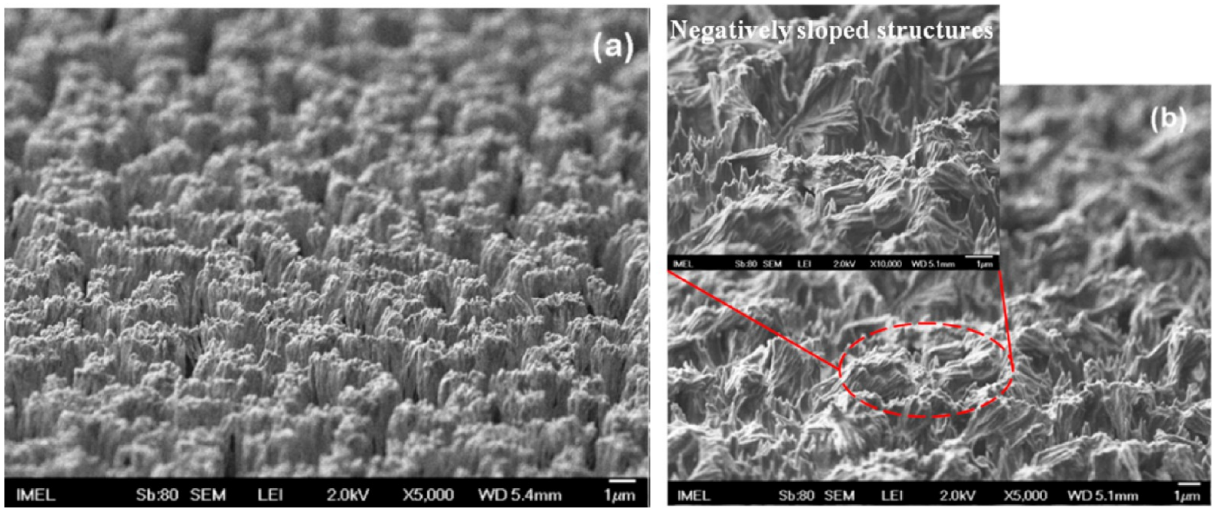

Figure 6. SEM images of 10 min SF_6 plasma-textured PDMS surfaces (a) before silanization and (b) after silanization.

min plasma processing is shown in Figure 6a. These surfaces are not stable upon water immersion. However, a subsequent silanization in cyclohexane is used for the stabilization of the topography, yielding the surface in Figure 6b (see also Supporting Information Figure S3). Similar results for the stabilization of the topography have been also observed for other polymer surfaces, and will be reported elsewhere.

The filamental topography produced after several minutes of plasma texturing (section 2.5) enhances the resulting oleophobicity. For example, the soya oil static contact angle upon texturing for 10 min becomes 152°. PDMS exhibits curved grass-like negatively sloped structures after the silanization (Figure 6b), but the resulting surface is less homogeneous than PMMA and PEEK. Notice the topography differentiation before and after silanization: vertical pillars (Figure 6a) bend upon grafting (Figure 6b), thus exhibiting the advantageous negatively sloped profile needed for super-amphiphobicity. As an overall result, fluorosilanized PDMS exhibits a slightly lower CA with hexadecane than fluorosilanized PMMA and PEEK, due to the observed surface inhomogeneity, as indicated above. The static and advancing contact angle and the hysteresis for water, soya oil, and hexadecane are shown in Table 5.

3.3. Scratch, Hydrolytic, and Hexadecane Resistance of FDTS-Modified Polymeric Surfaces. For practical applications of such monolayer-coated polymeric surfaces, either in outdoor uses or inside microchannels, it is important that both the surface morphology and the monolayer are stable upon immersion in various probe liquids, as well as upon application of mechanical forces due to scratching or water drag forces. In the following sections, the surfaces are characterized with respect to those two properties using hydrolytic and hexadecane immersion stability tests and nanoscratch tests.

Table 5. Static, Advancing, and Receding Contact Angles for Water, Soya Oil, and Hexadecane on Perfluorosilane-Modified Hierarchical Randomly Rough PDMS Surfaces (in degrees)[a]

liquid	contact angle	PDMS 10 min SF_6 plasma
water	static	167°
	adv/rec	168°/165° (3°)
soya oil	static	152°
	adv/rec	157°/145° (12°)
hexadecane	static	135°
	adv/rec	142°/129° (13°)

[a]5 μL liquid; uncertainty in static CA, ±2°; receding CA, ±5°.

3.3.1. Hydrolytic and Hexadecane Immersion Stability Test of FDTS Modified Flat Nonplasma Textured Surfaces. In order to study the stability of the attached monolayers in various liquids, monolayer-coated polymers were immersed in continuously flowing deionized water and agitated hexadecane. Contact angles for three probe liquids (namely, 1, water; 2, soya oil; 3, hexadecane) were monitored for a period of two weeks.

Figure 7 shows that all polymer surfaces exhibit good hydrolytic and hexadecane stability. Contact angles for three probing liquids, and hysteresis remain practically constant over a period of two week immersion in water or in hexadecane.

However, longer hydrolytic stability tests (40 days; see Supporting Information) revealed that PEEK shows slightly deteriorating stability compared to stable PMMA and PDMS. We suspect that there are two main factors for the lower stability of PEEK in the prolonged hydrolytic tests: First, it is possible that not enough surface OH groups are generated by the plasma reactivation step on this polymer. Second, it is known that PEEK is not attacked by cyclohexane, while PMMA[61] and PDMS[62] are affected and probably slightly swelled by the solvent. We thus expect that silanization of PMMA and PDMS could extend a few nanometers from the surface into the swollen layer. Further swelling will not happen, since the multifunctional silylating agent causes cross-linking on the surface. This surface-only swelling and silylation would make that layer more stable in hydrolysis, by analogy to surface silylation of photoresists, which become stable (unetchable) in oxygen plasmas.[63]

3.3.2. Hydrolytic and Hexadecane Immersion Stability Test of FDTS Modified Plasma Textured Surfaces. Figure 8 presents the advancing and receding CAs of water, soya oil, and hexadecane on perfluorosilane-modified, hierarchical, plasma-textured surfaces immersed in two different liquids, water (red bars) and hexadecane (green bars), for a period of two weeks. Figure 8A shows hydrolytic and hexadecane immersion stability for PMMA. The advancing and receding CAs for all probe liquids changed very little upon immersion in water for 14 days.

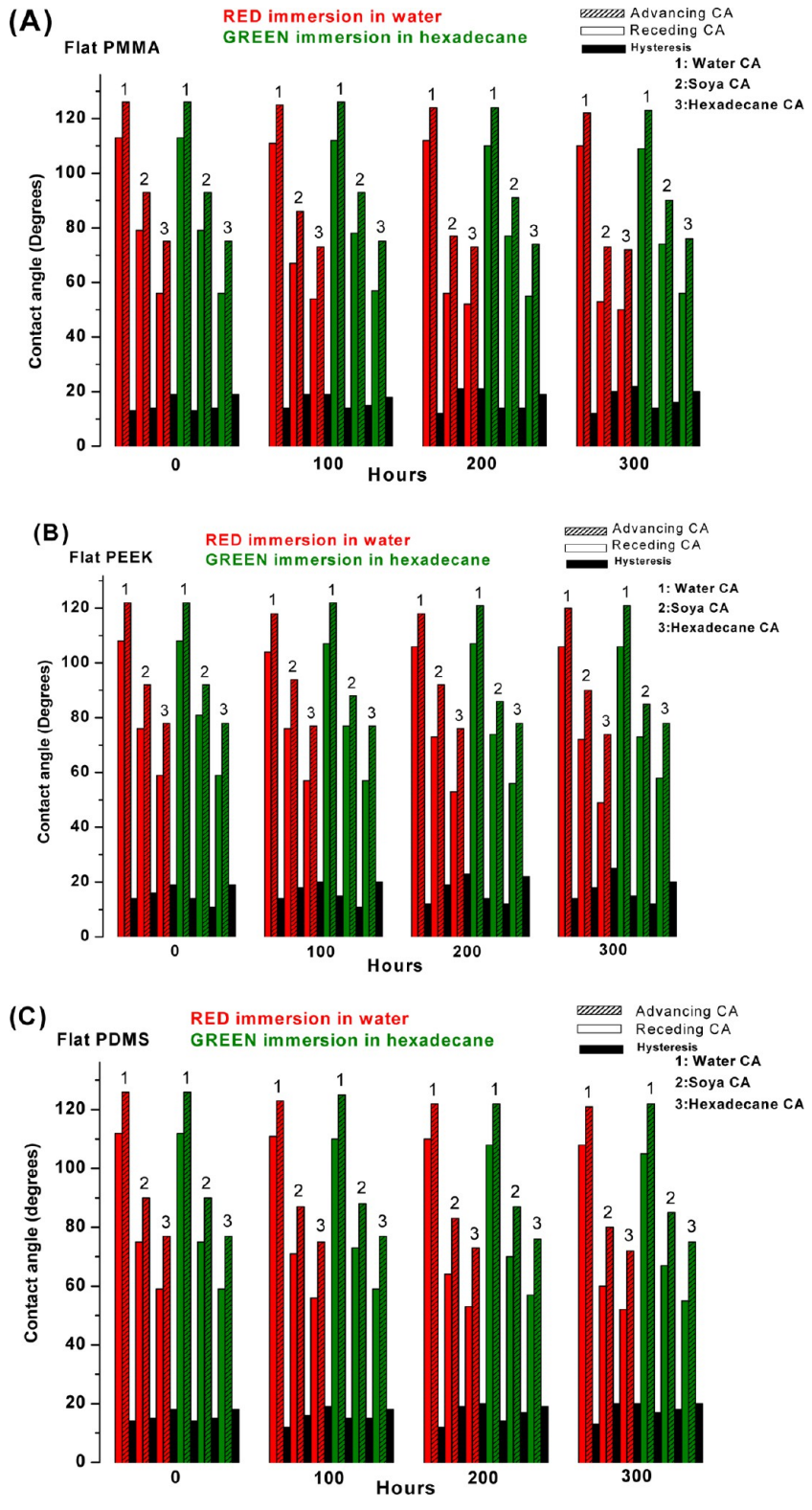

Figure 7. Hydrolytic and hexadecane immersion stability tests for perfluorinated SAM on flat surfaces. Advancing (hatched red or green bar), receding (filled red or green bar) CA, and hysteresis (black bar) are shown for water, soya oil, and hexadecane on flat nonplasma textured surfaces of (A) PMMA, (B) PEEK, and (C) PDMS after immersion in water (red bars) and hexadecane (green bars).

Hysteresis for hexadecane increased only by 2−4°, moving from just below to just above the threshold of 10°, i.e., at the border of superamphiphobicity. Immersion in hexadecane showed a similar trend for all liquids. Thus, the 20 min textured PMMA surface shows a high resistance to both water and hexadecane immersion, demonstrating stable superhydrophobic and highly oleophobic properties for hexadecane drops. This implies that the SAM is well packed over the whole surface and acts as a very good barrier to prevent water or

dx.doi.org/10.1021/am5000432 | ACS Appl. Mater. Interfaces 2014, 6, 6510−6524

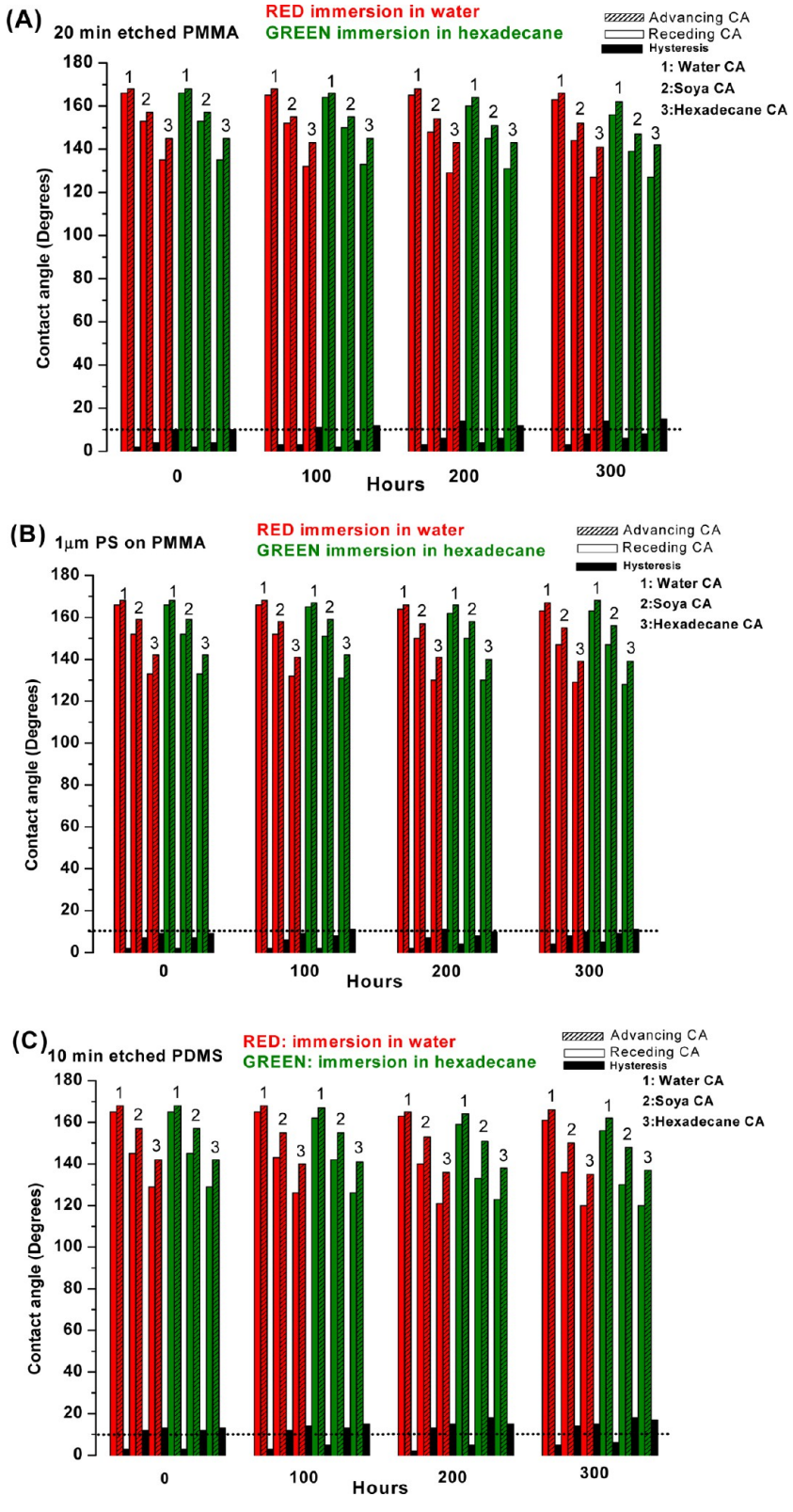

Figure 8. Hydrolytic and hexadecane immersion stability tests of perfluorinated SAM on plasma textured polymeric surfaces. Advancing (hatched red or green bar), receding (filled red or green bar) CA, and hysteresis (black bar) are shown for water, soya oil, and hexadecane on different plasma textured polymeric surfaces: (A) 20 min plasma textured PMMA; (B) PMMA surfaces masked with 1 μm PS microparticles and plasma textured; (C) 10 min plasma-textured PDMS. The ten degree hysteresis limit for superamphiphobicity is shown with dotted line.

hexadecane from damaging the Si−O−C bond that links the monolayer to the substrate.

Figure 8B shows hydrolytic and hexadecane immersion stability for ordered plasma-textured PMMA surfaces (using 1 PS particles as etch masks) demonstrating stable super-

dx.doi.org/10.1021/am5000432 | ACS Appl. Mater. Interfaces 2014, 6, 6510−6524

amphiphobicity. The advancing and receding CAs for all probe liquids practically did not change upon immersion in water for 14 days. Immersion in hexadecane showed a similar trend for all liquids. Thus, the ordered hierarchical PMMA surface also shows an excellent resistance to water and hexadecane immersion, demonstrating stable superhydrophobicity and superamphiphobicity. We suspect that the multiscale roughness and the overhanging pillar shape slightly enhances amphiphobicity and stability compared to the randomly rough surfaces allowing hysteresis to remain just below the border of 10°, i.e., remain superamphiphobic.

Figure 8C shows the hydrolytic and hexadecane immersion stability for PDMS. This surface is at the border of superamphiphobicity before immersion, and immersion tests increase the hysteresis for those two liquids from 2° to 4°. Thus, these surfaces maintain superhydrophobicity and oleophobicity. In practice, PDMS retains its oleophobic and superhydrophobic properties presented in Table 5.

We note that we have also performed longer hydrolytic stability tests (40 days) shown in Supporting Information Figure S8. The tests show that with the exception of PEEK all surfaces remain superhydrophobic with small changes in CA and hysteresis.

3.3.3. FDTS Coating Wear Resistance. To investigate the wear resistance of the FDTS-coated polymer surfaces, we first performed scratch tests on 2 min O_2 textured PMMA surfaces. These surfaces have enough topography to be superhydrophobic, but are not superamphiphobic.[45] Thus, they can give information for both the conformality of the coating on a small nanotexture, while being intermediate to the flat air plasma-activated PMMA (section 3.1), and the very rough 20 min textured PMMA. PMMA substrate was chosen due to the optimum hydrolytic stability exhibited (Figures 7 and 8A,B).

The scratch test result (Figure 9) shows CoF values during both the scratch and postscratch part of the cycle for the FDTS-coated PMMA that are 50% lower than that for the uncoated PMMA. The average CoF for the uncoated PMMA is 0.4 and becomes 0.2 after grafting with FDTS. Coefficients are identical in the scratch and postscratch part of the cycle, implying that the coating is not detached or destroyed for loads up to 80 μN. This also implies that the coating acts as lubricant on the surface, an argument that is highlighted in the following section.

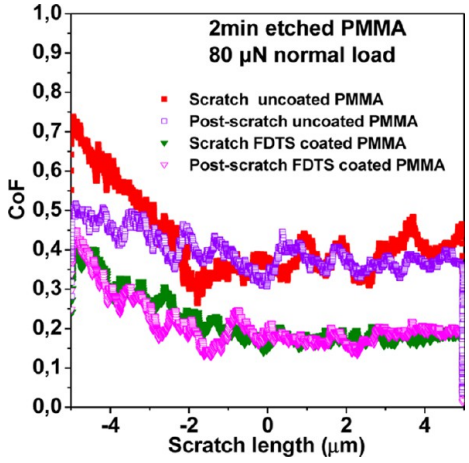

Figure 9. Coefficient of friction as a function of scratch path, for 2 min textured uncoated and FDTS coated PMMA samples. The load during the scratch test is 80 μN. Notice the identical CoF in both cases during scratch and postscratch (duplicate scratch on the same line) and the lower CoF for FDTS coated samples.

3.3.4. Scratch Resistance of the PS/PMMA Surfaces. Here, we perform scratch tests on the 1 μm PS/PMMA ordered pillar surface in order to test the wear of the micro-nanostructures and the FDTS coating on them. The PS/PMMA pillar surface was chosen due to its order compared to the random textured surfaces, and due to its optimized wetting characteristics. Figure 10a shows an example of the CoF obtained from the scratch and postscratch test on uncoated PS/PMMA samples for a 85 μN load. Notice that the tip starts sliding into and out of the spacing between the micropillars, which results in a lower friction when it slides in, and a higher friction when it travels out in order to deform the micropillar.[64,65] We note that the Berkovich tip is a blunt tip with an opening angle of 76.9° and 65.3°, and thus it is a not similar to a sharp AFM tip capable of faithfully probing the topography of the interpillar space. Despite the size of the tip, the tip motion yields a CoF fluctuation that follows the shape of the surface morphology, as presented in Figure 10a. Figure 10a also emphasizes the scratch resistance of the ordered 1 μm PS/PMMA pillars during duplicate scratching (i.e., scratch and postscratch). The pillars are not destroyed by the tip motion during the scratch step, and the fluctuation that follows the topography remains during the postscratch for loads up to 85 μN. This behavior has also been observed by Bo et al., who measured the CoF of microtextured poly(dimethylsiloxane) at both microscale and macroscale.[36] This reversible behavior upon scratching of textured surfaces has been attributed to the comparable size of the pillars to the interpillar spacings.[64,65] The scratch resistance of the pillars is in agreement with approximate calculations referred to in section 2.8, which indicate that the Young modulus and the critical buckling load of the pillars are not exceeded.

Figure 10b shows the nanoscratch test for the FDTS coated PS/PMMA pillars. The CoF values for FDTS-coated PS/PMMA are again 50% lower than the uncoated PS/PMMA system, and they are similar in the scratch and postscratch part of the cycle, highlighting again the excellent coating adhesion onto the surface (see also section 3.3.3). In the FDTS-coated PS/PMMA surface (Figure 10b) the tip motion yields a CoF fluctuation that does not follow the shape of the pillar geometry. This implies that the FDTS coating acts as lubricant when deposited on the surface.

Recently, Zhao et al.[17] suggested that the choice of the pillar diameter to height ratio should depend on the application and the compromise between structural and wetting stability. Although this is generally accepted, careful structural design and coating adhesion optimization can lead to surfaces, in which wetting property optimization does not compromise structural stability and scratch resistance. Indeed, we show that the method developed in this work resulted in surfaces that are scratch resistant and simultaneously hydrolytically and hexadecane-immersion stable for a long period.

Average (of scratch and postscratch) CoF values for different loads are shown in the Supporting Information (Figure S6). Averaging the CoF data from both parts of the cycle (scratch and postscratch) results in better visualization (fluctuation that follows the topography) of the pillar shape and periodicity.

To further verify the scratch resistance of the structures, we studied their morphology in the scratched area using SEM imaging (see Figure 11). Nine 10-μm-long constant load scratches (three for every load 40, 60, 80 μN) and two longer

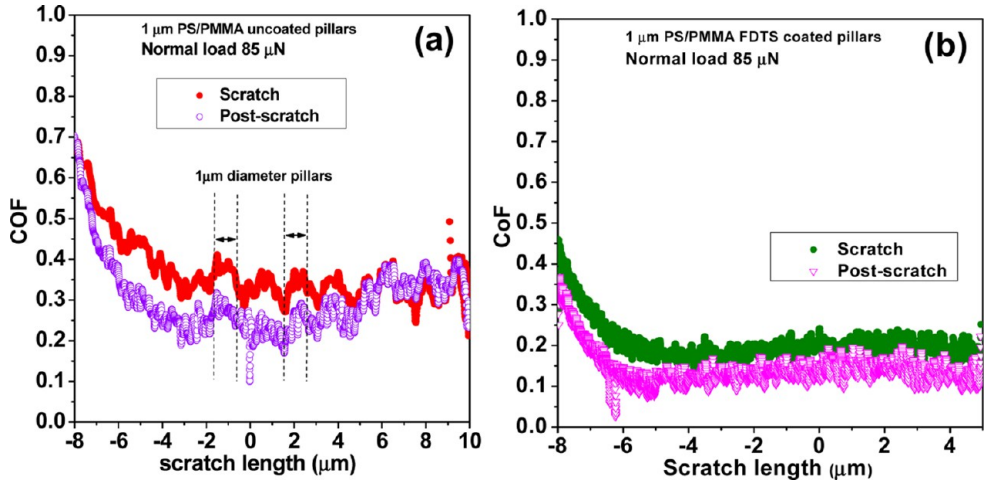

Figure 10. Coefficient of friction as a function of scratch path during scratch and postscratch: (a) for uncoated and (b) FDTS coated 1 μm PS/PMMA samples.

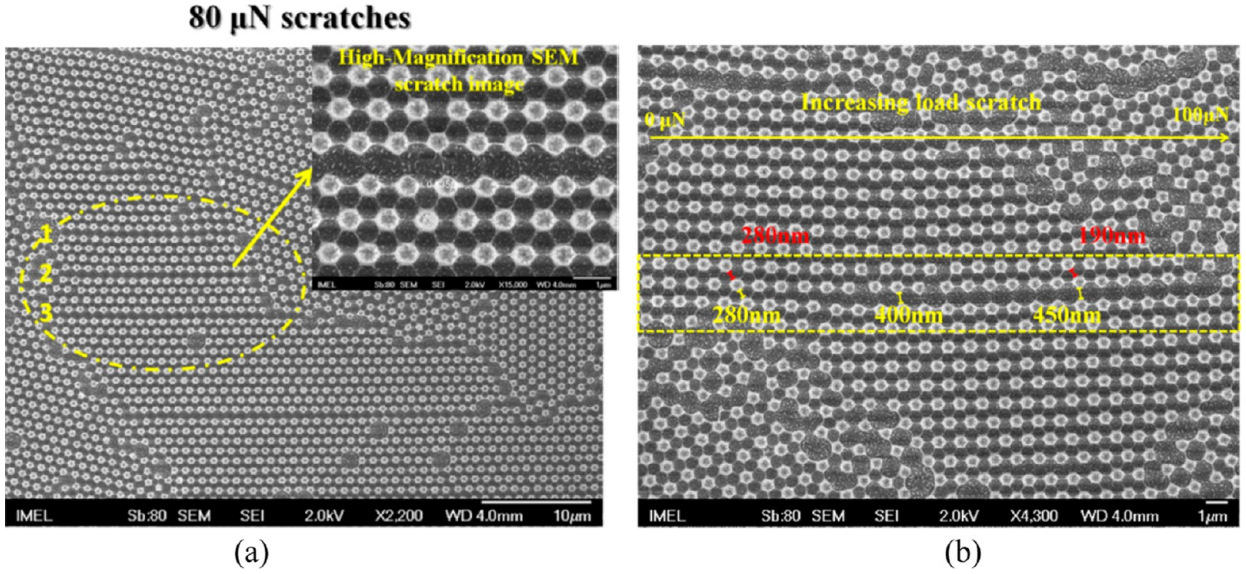

Figure 11. Top-down SEM images after the scratch test. (a) For constant loads of 40, 60, 80 μN. Only 80 μN scratches are observable, and show a slight increase of the interpillar distance as the large tip pushes them aside. (b) For increasing load from 0 to 100 μN. Notice the increase in the interpillar distance (as the load increases across the scratch) from 280 to 450 nm (yellow lines), that is followed by the analogous decrease in the neighboring pillars from 280 to 190 nm (red lines).

(~40 μm) increasing load scratches were performed in a premarked surface area (to facilitate scratch location with the SEM if observable). Then, the samples were observed in SEM in an effort to image possible surface damage from the scratches.

As expected from the results about the CoF measurement, structures were not detached or destroyed during the scratch even after duplicate scratching. SEM images in Figure 11a show that 80 μN scratches have only slightly pushed aside the pillars and increased the interpillar distance due to the deeper penetration of the large tip, while smaller load (40 and 60 μN) scratches could not even be detected. Therefore, these smaller loads do not affect the structures (see Figure 11). We emphasize that this minimal interpillar distance increase has no or minimal effect on the surface wettability when compared with the usual dislocation defects that are present on the sample surface after the colloidal self-assembly before any scratch test. This minimal interpillar distance increase, when scratching with 85 μN, may be the cause of the slightly reduced CoF shown in Figure 10 during the second scan; this reduction of the CoF is almost at the border of the measurement error.

An increasing load scratch test was also done as described in section 2.8 to help in understanding the effect of different loads on the scratch resistance of the pillars. Figure 11b shows that the interpillar distance increases as the load increases and the tip penetrates deeper, but again no collapse or destruction or buckling is observed up to 100 μN load used in this study. We want to emphasize that the maximum load we used (~100 μN) corresponds to stresses of some GPa, which are below the Young's modulus, and below the critical buckling load of a pillar confirming the theoretical calculations in section 2.8.

The nanomechanical tests presented above allowed us to probe the scratch resistance of both the individual nanostructures on the polymer and their FDTS coating. We have seen the range of scratch forces, which cause less damage compared to the defects already existing on the surface itself. However,

dx.doi.org/10.1021/am5000432 | ACS Appl. Mater. Interfaces 2014, 6, 6510−6524

due to the limited area of the scratch, compared to the size of a water drop, effects on the contact angle cannot be measured with our test, although minimal are expected.

It is therefore difficult to convert our results to macro-mechanical testing such as abrasion tests, where a large surface is affected, and the effects on the contact angle are immediately obvious. We plan to conduct such tests in the near future, and compare the nano and micromechanical measurements.

4. CONCLUSIONS

We have developed a simple and generic method to produce superhydrophobic and superamphiphobic toward superoleophobic polymeric surfaces that display long-term stability in water and hexadecane, and scratch resistance. Our approach involves two steps: (1) hierarchical micro-nanotexturing of the surfaces (PEEK, PMMA, and PDMS) by a plasma-etching step—especially when plasma texturing is performed using as a mask a self-assembled layer of monodisperse micrometer-sized particles, this yields an ordered micro and nanotextured surface structure—(2) grafting of these etched surfaces with a perfluorosilane, which yields superamphiphobic polymeric surfaces. Such surfaces display a long-term (14 days) hydrolytic/hexadecane stability, as indicated by immersion measurements in water and hexadecane. Longer hydrolytic stability tests show stable superhydrophobic behavior for a period of >40 days. Furthermore, nanoscratch experimental results show the excellent coating adhesion and good scratch resistance of the ordered micro and nanotextured pillar structures. This simple approach will allow the construction of a wide range of superamphiphobic surfaces, which can be applied in MEMS, microfluidics, (bio-) sensor devices, and outdoor applications.

■ ASSOCIATED CONTENT

Supporting Information

Additional information about XPS analysis, hydrolytic stability setup, silinization effect on the surfaces, tribological data and long-term (40 days) hydrolytic stability tests. Two videos on rolling-off movements. This material is available free of charge via the Internet at http://pubs.acs.org.

■ AUTHOR INFORMATION

Corresponding Authors

*Fax:+30-210-6503237, Tel: +30-210-6503237, E-mail: evgog@imel.demokritos.gr.

*Tel: +31-317-482361, E-mail: Han.Zuilhof@wur.nl.

Author Contributions

K. Ellinas and S. Pujari contributed equally.

Notes

The authors declare no competing financial interest.

■ ACKNOWLEDGMENTS

We thank Marcel Giesbers and Barend van Lagen for instrumental assistance, and Arun Kumar Gnanappa and Cees van Rijn for initiating these experiments. This project is partially funded by the Marie Curie European Union FP7 project "Surface Physics for Advanced Materials", by ASML, The Netherlands, and by Hellenic and European Regional Development Funds (ERDF) under the Hellenic National Strategic Reference Framework (NSRF) 2007-2013, of the Project "THALIS-DESIgn and fabrication of Robust supErhyDROPhobic/philic surfaces and their application in the realization of "smart" microfluidic valves".

■ REFERENCES

(1) Li, X.-M.; Reinhoudt, D.; Crego-Calama, M. What Do We Need for a Superhydrophobic Surface? A Review on the Recent Progress in the Preparation of Superhydrophobic Surfaces. *Chem. Soc. Rev.* **2007**, *36* (8), 1350−1368.

(2) Wong, T.-S.; Sun, T.; Feng, L.; Aizenberg, J. Interfacial Materials with Special Wettability. *MRS Bull.* **2013**, *38* (05), 366−371.

(3) Bellanger, H.; Darmanin, T.; Taffin de Givenchy, E.; Guittard, F. Chemical and Physical Pathways for the Preparation of Superoleophobic Surfaces and Related Wetting Theories. *Chem. Rev.* **2014**, DOI: 10.1021/cr400169m.

(4) Liu, K.; Tian, Y.; Jiang, L. Bio-Inspired Superoleophobic and Smart Materials: Design, Fabrication, and Application. *Prog. Polym. Sci.* **2012**, *58* (4), 503−564.

(5) Tuteja, A.; Choi, W.; Ma, M.; Mabry, J. M.; Mazzella, S. A.; Rutledge, G. C.; McKinley, G. H.; Cohen, R. E. Designing Superoleophobic Surfaces. *Science* **2007**, *318* (5856), 1618−1622.

(6) Tsougeni, K.; Papageorgiou, D.; Tserepi, A.; Gogolides, E. "Smart" Polymeric Microfluidics Fabricated by Plasma Processing: Controlled Wetting, Capillary Filling and Hydrophobic Valving. *Lab Chip* **2010**, *10* (4), 462−469.

(7) Tanzi, S.; Østergaard, P. F.; Matteucci, M.; Christiansen, T. L.; Cech, J.; Marie, R.; Taboryski, R. Fabrication of Combined-Scale Nano- and Microfluidic Polymer Systems Using a Multilevel Dry Etching, Electroplating and Molding Process. *J. Micromech. Microeng.* **2012**, *22* (11), 115008.

(8) Vourdas, N.; Tserepi, A.; Boudouvis, A. G.; Gogolides, E. Plasma Processing for Polymeric Microfluidics Fabrication and Surface Modification: Effect of Super-Hydrophobic Walls on Electroosmotic Flow. *Microelectron. Eng.* **2008**, *85* (5−6), 1124−1127.

(9) Zhao, H.; Law, K.-Y.; Sambhy, V. Fabrication, Surface Properties, and Origin of Superoleophobicity for a Model Textured Surface. *Langmuir* **2011**, *27* (10), 5927−5935.

(10) Ellinas, K.; Tserepi, A.; Gogolides, E. Superhydrophobic, Passive Microvalves with Controllable Opening Threshold: Exploiting Plasma Nanotextured Microfluidics for a Programmable Flow Switchboard. *Microfluid. Nanofluid.* **2014**, DOI: 10.1007/s10404-014-1335-9.

(11) Pujari, S. P.; Spruijt, E.; Stuart, M. A. C.; Rijn, C. J. M. v.; Paulusse, J. M. J.; Zuilhof, H. Ultra-Low Adhesion and Friction of Fluoro-Hydro Alkyne-Derived Self-Assembled Monolayers on H-Terminated Si(111). *Langmuir* **2012**, *28*, 17690−17700.

(12) Mabry, J. M.; Vij, A.; Iacono, S. T.; Viers, B. D. Fluorinated Polyhedral Oligomeric Silsesquioxanes (F-Poss). *Angew. Chem., Int. Ed.* **2008**, *120* (22), 4205−4208.

(13) Pujari, S. P.; Spruijt, E.; Cohen Stuart, M. A.; van Rijn, C. J.; Paulusse, J. M. J.; Zuilhof, H. Ultra-Low Adhesion and Friction of Fluoro-Hydro Alkyne-Derived Self-Assembled Monolayers on H-Terminated Si(111). *Langmuir* **2012**, *28* (51), 17690−17700.

(14) Kota, A. K.; Choi, W.; Tuteja, A. Superomniphobic Surfaces: Design and Durability. *MRS Bull.* **2013**, *38* (05), 383−390.

(15) Butt, H.-J.; Semprebon, C.; Papadopoulos, P.; Vollmer, D.; Brinkmann, M.; Ciccotti, M. Design Principles for Superamphiphobic Surfaces. *Soft Matter* **2013**, *9* (2), 418−428.

(16) Kota, A. K.; Li, Y.; Mabry, J. M.; Tuteja, A. Hierarchically Structured Superoleophobic Surfaces with Ultralow Contact Angle Hysteresis. *Adv. Mater.* **2012**, *24* (43), 5838−5843.

(17) Zhao, H.; Park, K.-C.; Law, K.-Y. Effect of Surface Texturing on Superoleophobicity, Contact Angle Hysteresis, and "Robustness". *Langmuir* **2012**, *28* (42), 14925−14934.

(18) Sheen, Y.-C.; Huang, Y.-C.; Liao, C.-S.; Chou, H.-Y.; Chang, F.-C. New Approach to Fabricate an Extremely Super-Amphiphobic Surface Based on Fluorinated Silica Nanoparticles. *J. Polym. Sci., Part B* **2008**, *46* (18), 1984−1990.

(19) Tuteja, A.; Choi, W.; Mabry, J. M.; McKinley, G. H.; Cohen, R. E. Robust Omniphobic Surfaces. *Proc. Natl. Acad. Sci. U.S.A.* **2008**, *105* (47), 18200−18205.

(20) Zhao, H.; Law, K.-Y. Directional Self-Cleaning Superoleophobic Surface. *Langmuir* **2012**, *28* (32), 11812−11818.

(21) Pan, S.; Kota, A. K.; Mabry, J. M.; Tuteja, A. Superomniphobic Surfaces for Effective Chemical Shielding. *J. Am. Chem. Soc.* **2013**, *135* (2), 578−581.
(22) Xue, Z.; Liu, M.; Jiang, L. Recent Developments in Polymeric Superoleophobic Surfaces. *J. Polym. Sci., Part B: Polym. Phys.* **2012**, *50* (17), 1209−1224.
(23) Gnanappa, A. K.; Papageorgiou, D. P.; Gogolides, E.; Tserepi, A.; Papathanasiou, A. G.; Boudouvis, A. G. Hierarchical, Plasma Nanotextured, Robust Superamphiphobic Polymeric Surfaces Structurally Stabilized through a Wetting−Drying Cycle. *Plasma Processes Polym.* **2012**, *9* (3), 304−315.
(24) Ellinas, K.; Tserepi, A.; Gogolides, E. From Superamphiphobic to Amphiphilic Polymeric Surfaces with Ordered Hierarchical Roughness Fabricated with Colloidal Lithography and Plasma Nanotexturing. *Langmuir* **2011**, *27* (7), 3960−3969.
(25) Waite, J. H. Nature's Underwater Adhesive Specialist. *Int. J. Adhes. Adhes.* **1987**, *7* (1), 9−14.
(26) Lindner, E.; Arias, E. Surface Free Energy Characteristics of Polyfluorinated Silane Films. *Langmuir* **1992**, *8* (4), 1195−1198.
(27) Zimmermann, J.; Rabe, M.; Artus, G. R. J.; Seeger, S. Patterned Superfunctional Surfaces Based on a Silicone Nanofilament Coating. *Soft Matter* **2008**, *4* (3), 450−452.
(28) Pujari, S. P.; Scheres, L.; Weidner, T.; Baio, J. E.; Cohen Stuart, M. A.; van Rijn, C. J. M.; Zuilhof, H. Covalently Attached Organic Monolayers onto Silicon Carbide from 1-Alkynes: Molecular Structure and Tribological Properties. *Langmuir* **2013**, *29* (12), 4019−4031.
(29) Lee, S.; Park, J.-S.; Lee, T. R. The Wettability of Fluoropolymer Surfaces: Influence of Surface Dipoles. *Langmuir* **2008**, *24* (9), 4817−4826.
(30) Brown, L.; Koerner, T.; Horton, J. H.; Oleschuk, R. D. Fabrication and Characterization of Poly(Methylmethacrylate) Microfluidic Devices Bonded Using Surface Modifications and Solvents. *Lab Chip* **2006**, *6* (1), 66−73.
(31) Bhushan, B.; Hansford, D.; Lee, K. K. Surface Modification of Silicon and Polydimethylsiloxane Surfaces with Vapor-Phase-Deposited Ultrathin Fluorosilane Films for Biomedical Nanodevices. *J. Vac. Sci. Technol., A* **2006**, *24* (4), 1197−1202.
(32) Chandra, D.; Yang, S. Stability of High-Aspect-Ratio Micropillar Arrays against Adhesive and Capillary Forces. *Acc. Chem. Res.* **2010**, *43* (8), 1080−1091.
(33) Deng, X.; Mammen, L.; Butt, H.-J.; Vollmer, D. Candle Soot as a Template for a Transparent Robust Superamphiphobic Coating. *Science* **2012**, *335* (6064), 67−70.
(34) Wang, H.; Xue, Y.; Ding, J.; Feng, L.; Wang, X.; Lin, T. Durable, Self-Healing Superhydrophobic and Superoleophobic Surfaces from Fluorinated-Decyl Polyhedral Oligomeric Silsesquioxane and Hydrolyzed Fluorinated Alkyl Silane. *Angew. Chem., Int. Ed.* **2011**, *50* (48), 11433−11436.
(35) Su, C.; Xu, Y.; Gong, F.; Wang, F.; Li, C. The Abrasion Resistance of a Superhydrophobic Surface Comprised of Polyurethane Elastomer. *Soft Matter* **2010**, *6* (24), 6068−6071.
(36) He, B.; Chen, W.; Wang, Q. J. Surface Texture Effect on Friction of a Microtextured Poly(Dimethylsiloxane) (Pdms). *Tribol. Lett.* **2008**, *31* (3), 187−197.
(37) Pujari, S. P.; Zuilhof, H. Highly Wear-Resistant Ultra-Thin Per-Fluorinated Organic Monolayers on Silicon(1 1 1) Surfaces. *Appl. Surf. Sci.* **2013**, *287*, 159−164.
(38) Skarmoutsou, A.; Charitidis, C. A.; Gnanappa, A. K.; Tserepi, A.; Gogolides, E. Nanomechanical and Nanotribological Properties of Plasma Nanotextured Superhydrophilic and Superhydrophobic Polymeric Surfaces. *Nanotechnology* **2012**, *23* (50), 505711.
(39) Ellinas, K.; Smyrnakis, A.; Malainou, A.; Tserepi, A.; Gogolides, E. "Mesh-Assisted" Colloidal Lithography and Plasma Etching: A Route to Large-Area, Uniform, Ordered Nano-Pillar and Nanopost Fabrication on Versatile Substrates. *Microelectron. Eng.* **2011**, *88* (8), 2547−2551.
(40) Tsougeni, K.; Vourdas, N.; Tserepi, A.; Gogolides, E.; Cardinaud, C. Mechanisms of Oxygen Plasma Nanotexturing of Organic Polymer Surfaces: From Stable Super Hydrophilic to Super Hydrophobic Surfaces. *Langmuir* **2009**, *25* (19), 11748−11759.
(41) Kokkoris, G.; Gogolides, E. The Potential of Ion-Driven Etching with Simultaneous Deposition of Impurities for Inducing Periodic Dots on Surfaces. *J. Phys. D: Appl. Phys.* **2012**, *45* (16).
(42) Tserepi, A. G. E.; Misiakos, K.; Vlachopoulou, M-E.; Vourdas, N. Method for the Fabrication of High Surface Area Ratio and High Aspect Ratio Surfaces on Substrates. PCT/GR2006/000011, 2006.
(43) Vlachopoulou, M.-E.; Kokkoris, G.; Cardinaud, C.; Gogolides, E.; Tserepi, A. Plasma Etching of Poly(Dimethylsiloxane): Roughness Formation, Mechanism, Control, and Application in the Fabrication of Microfluidic Structures. *Plasma Processes Polym.* **2013**, *10* (1), 29−40.
(44) Tsougeni, K.; Petrou, P. S.; Tserepi, A.; Kakabakos, S. E.; Gogolides, E. Nano-Texturing of Poly(Methyl Methacrylate) Polymer Using Plasma Processes and Applications in Wetting Control and Protein Adsorption. *Microelectron. Eng.* **2009**, *86* (4−6), 1424−1427.
(45) Vourdas, N.; Tserepi, A.; Gogolides, E. Nanotextured Super-Hydrophobic Transparent Poly(Methyl Methacrylate) Surfaces Using High-Density Plasma Processing. *Nanotechnology* **2007**, *18* (12), 125304.
(46) Accardo, A.; Gentile, F.; Mecarini, F.; De Angelis, F.; Bughammer, M.; Di Fabrizio, E.; Riekel, C. In Situ X-Ray Scattering Studies of Protein Solution Droplets Drying on Micro- and Nanopatterned Superhydrophobic Pmma Surfaces. *Langmuir* **2010**, *26* (18), 15057−15064.
(47) Di Mundo, R.; Palumbo, F.; d'Agostino, R. Influence of Chemistry on Wetting Dynamics of Nanotextured Hydrophobic Surfaces. *Langmuir* **2010**, *26* (7), 5196−5201.
(48) Charitidis, C. A.; Dragatogiannis, D. A.; Koumoulos, E. P.; Kartsonakis, I. A. Residual Stress and Deformation Mechanism of Friction Stir Welded Aluminum Alloys by Nanoindentation. *Mater. Sci. Eng., A* **2012**, *540*, 226−234.
(49) Koumoulos, E. P.; Charitidis, C. A.; Papageorgiou, D. P.; Papathanasiou, A. G.; Boudouvis, A. G. Nanomechanical and Nanotribological Properties of Hydrophobic Fluorocarbon Dielectric Coating on Tetraethoxysilane for Electrowetting Applications. *Surf. Coat. Technol.* **2012**, *206* (19−20), 3823−3831.
(50) Zeniou, A.; Ellinas, K.; Olziersky, A.; Gogolides, E. Ultra-High Aspect-Ratio Si Nanowires Fabricated with Plasma Etching: Plasma Processing, Mechanical Stability Analysis against Adhesion and Capillary Forces and Oleophobicity. *Nanotechnology* **2013**, *25* (3), 035302.
(51) Beamson, G.; Briggs, D. *High Resolution XPS of Organic Polymers: The Scienta Esca300 Database*; John Wiley & Sons, 1992.
(52) Lenk, T. J.; Hallmark, V. M.; Hoffmann, C. L.; Rabolt, J. F.; Castner, D. G.; Erdelen, C.; Ringsdorf, H. Structural Investigation of Molecular Organization in Self-Assembled Monolayers of a Semi-fluorinated Amidethiol. *Langmuir* **1994**, *10* (12), 4610−4617.
(53) Gao, L.; McCarthy, T. J. Contact Angle Hysteresis Explained. *Langmuir* **2006**, *22* (14), 6234−6237.
(54) Shibuichi, S.; Yamamoto, T.; Onda, T.; Tsujii, K. Super Water- and Oil-Repellent Surfaces Resulting from Fractal Structure. *J. Colloid Interface Sci.* **1998**, *208* (1), 287−294.
(55) Onda, T.; Shibuichi, S.; Satoh, N.; Tsujii, K. Super-Water-Repellent Fractal Surfaces. *Langmuir* **1996**, *12* (9), 2125−2127.
(56) Zhang, J.; Li, J.; Han, Y. Superhydrophobic Ptfe Surfaces by Extension. *Macromol. Rapid Commun.* **2004**, *25* (11), 1105−1108.
(57) van de Grampel, R. D.; Ming, W.; Gildenpfennig, A.; Laven, J.; Brongersma, H. H.; de With, G.; van der Linde, R. Quantification of Fluorine Density in the Outermost Atomic Layer. *Langmuir* **2004**, *20* (1), 145−149.
(58) Song, X. Y.; Zhai, J.; Wang, Y. L.; Jiang, L. Fabrication of Superhydrophobic Surfaces by Self-Assembly and Their Water-Adhesion Properties. *J. Phys. Chem. B* **2005**, *109* (9), 4048−4052.
(59) Barriet, D.; Lee, T. R. Fluorinated Self-Assembled Monolayers: Composition, Structure and Interfacial Properties. *Curr. Opin. Colloid Interface Sci.* **2003**, *8* (3), 236−242.

(60) Li, L.; Breedveld, V.; Hess, D. W. Design and Fabrication of Superamphiphobic Paper Surfaces. *ACS Appl. Mater. Interfaces* **2013**, *5* (11), 5381−5386.
(61) Shen, J.-N.; Zheng, X.-C.; Ruan, H.-M.; Wu, L.-G.; Qiu, J.-H.; Gao, C.-J. Synthesis of Agcl/Pmma Hybrid Membranes and Their Sorption Performance of Cyclohexane/Cyclohexene. *J. Membr. Sci.* **2007**, *304* (1−2), 118−124.
(62) Hajsz, T.; Csetneki, I.; Filipcsei, G.; Zrinyi, M. Swelling Kinetics of Anisotropic Filler Loaded Pdms Networks. *Phys. Chem. Chem. Phys.* **2006**, *8* (8), 977−984.
(63) Kontziampasis, D.; Beltsios, K.; Tegou, E.; Argitis, P.; Gogolides, E. Optimized Surface Silylation of Chemically Amplified Epoxidized Photoresists for Micromachining Applications. *J. Appl. Polym. Sci.* **2010**, *117* (4), 2189−2195.
(64) Moseler, M.; Gumbsch, P.; Casiraghi, C.; Ferrari, A. C.; Robertson, J. The Ultrasmoothness of Diamond-Like Carbon Surfaces. *Science* **2005**, *309* (5740), 1545−1548.
(65) Gao, G. T.; Cannara, R. J.; Carpick, R. W.; Harrison, J. A. Atomic-Scale Friction on Diamond: A Comparison of Different Sliding Directions on (001) and (111) Surfaces Using Md and Afm. *Langmuir* **2007**, *23* (10), 5394−5405.